analytical chemistry

pubs.acs.org/ac Article

Effect and Mechanism of Deep Eutectic Solvents as Mobile-Phase Additives on Retention Behavior of G-Quadruplexes in Reversed-Phase High-Performance Liquid Chromatography

Lu-yan An, Long-yu Zhu, Min Zhu, Jun-qin Qiao,* Weijuan Zheng, Xiaojun Yao, and Hong-zhen Lian*

Cite This: *Anal. Chem.* 2026, 98, 16083−16095 Read Online

ACCESS | Metrics & More | Article Recommendations | Supporting Information

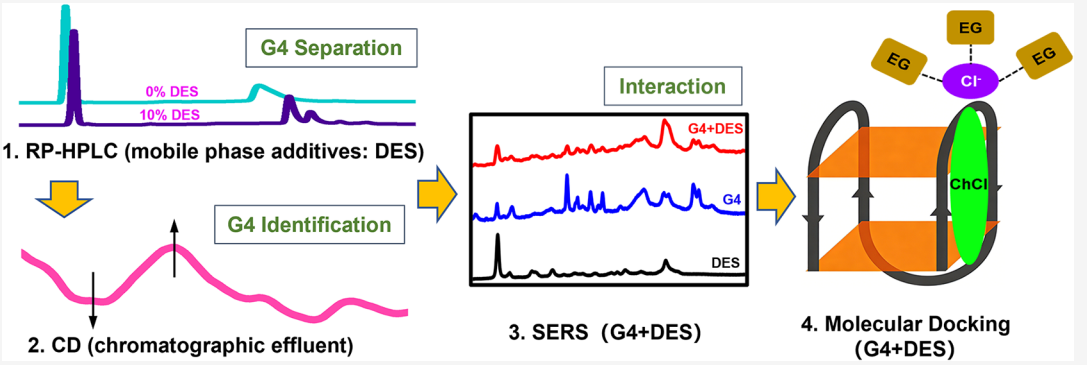

ABSTRACT: Separating complex biomolecules by liquid chromatography has always been challenging. In this work, deep eutectic solvents (DESs) were employed as mobile-phase additives to separate different G-quadruplex (G4) conformations using reversed-phase high-performance liquid chromatography (RP-HPLC). We investigated how different types and concentrations of DESs affected the retention behavior of G4s. The addition of DESs was found to significantly improve the peak shapes and resolution. At low concentrations, DESs enhanced the retention time of G4s, whereas higher concentrations led to a reduced retention. By combining circular dichroism analysis, we identified the G4 conformations corresponding to distinct chromatographic peaks and revealed that parallel G4 was more hydrophobic than nonparallel G4. In DESs, both hydrogen-bond donors and hydrogen-bond acceptors were shown to influence G4 retention behavior, with hydrogen-bond acceptors playing a dominant role. Using SERS and molecular docking, we further investigated the interaction mode between DESs and G4s to gain deeper insights into the retention mechanism. It showed that DESs interact with G4s through groove binding, supported by hydrogen bonding, cation-π, and electrostatic interactions, as well as electrostatic interaction toward the phosphate backbone, while DESs could also shield the silanol groups of the C18 stationary phase, thereby modulating the retention behavior of G4s. This work demonstrated that DESs, as promising green solvents, could effectively improve G4 separation in RP-HPLC. Notably, this is the first application of DESs in the liquid chromatographic separation of complex biological macromolecules.

INTRODUCTION

G-quadruplexes (G4s) are unique four-stranded structures formed by the folding of guanine-rich oligonucleotides. Four guanines are linked by Hoogsteen hydrogen bonds to form a G-quartet,[1] which is the fundamental building block of G4s. These G-quartets stack vertically to form the G4 structures, which are stabilized by cations (Na^+, K^+, and NH_4^+) located between the G-quartets.[2] G4s are found at telomeres and proto-oncogene promoters. Owing to their important roles in regulating gene transcription, G4s are promising targets for tumor therapy.[3] G4 structures show significant polymorphism,[4−11] and their biological functions are closely related to specific topological features.[12−16] Currently, a range of techniques are employed for analyzing G4 structures, including nuclear magnetic resonance,[17] single-crystal X-ray diffraction,[18] circular dichroism (CD),[19] ultraviolet spectroscopy,[20] fluorescence spectroscopy,[21] Raman spectroscopy,[22] and mass spectrometry analysis.[23] However, when multiple components coexist, these techniques face obvious difficulties in accurately characterizing the G4. In this case, the effective separation of mixed components is crucial.[24,25]

High-performance liquid chromatography (HPLC), as a common separation and analysis method, has been widely used

Received: December 26, 2025
Revised: May 17, 2026
Accepted: May 18, 2026
Published: May 22, 2026

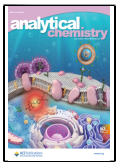

https://doi.org/10.1021/acs.analchem.5c08145
Anal. Chem. 2026, 98, 16083−16095

Table 1. G4-forming Sequences Involved in This Work

names	sequence (5′ to 3′)	descriptions	refs
TBA	GGTTGGTGTGGTTGG	thrombin-binding aptamer	59−62
24TTG	TTGGGTTAGGGTTAGGGTTAGGGA	human telomere	63,64
c-myc	TGAGGGTGGGTAGGGTGGGTAA	c-MYC promoter	65,66
GTERT-060	AGGGGAGGGGCTGGGAGGGC	human telomerase, hTERT promoter	67
12TAG	TAGGGTTAGGGT	human telomere	68
AS1411	GGTGGTGGTGGTTGTGGTGGTGGTGG	aptamer	69

Table 2. DESs Involved in This Work[a]

abbreviation	HBA	HBD	molar ratios	synthesis temperature (°C)	remarks
DES1	ChCl	EG	1:3	80	colorless, transparent, homogeneous solution
DES2	ChCl	EG	1:2	80	
DES3	ChCl	EG	1:3	60	
DES4	ChCl	EG	1:3	100	
DES5	ChCl	Urea	1:2	80	
DES6	ChCl	Gly	1:1	80	
DES7	ChCl	MA	1:2	80	
DES8	Betaine	EG	1:3	80	
DES9	TBAB	EG	1:3	80	
DES10	[BMIm][Br]	EG	1:3	80	

[a]ChCl: choline chloride, EG: ethylene glycol, Gly: glycerol, MA: malonic acid, TBAB: tetrabutylammonium bromide, and [BMIm][Br]: 1-butyl-3-methylimidazolium bromide.

in nucleic acid research.[26−28] The common chromatographic separation modes include ion-exchange chromatography (IEC),[29] affinity chromatography (AC),[30] size exclusion chromatography (SEC),[31] and ion-pair reversed-phase liquid chromatography (IP-RPLC).[32] Among them, IP-RPLC is the most widely used, attributed to its efficient separation. Our group had tried to use the classic IP-RPLC method for nucleic acid analysis to separate the different conformations of G4s but did not achieve good results. On the contrary, obviously better results were achieved by using the RP-HPLC method.[32] To improve the separation of various G4 conformations, our group further used ionic liquids as mobile-phase additives to improve the separation effect of G4s in RP-HPLC.[33] However, the environmental friendliness of ionic liquids has raised some concerns,[34] which may limit their long-term applicability.

Deep eutectic solvents (DESs) are systems consisting of mixtures of two or more compounds, which are usually obtained through strong interactions between hydrogen-bond donors (HBDs) and hydrogen-bond acceptors (HBAs).[35] Their melting points are apparently lower than the individual compound that makes up the DESs.[36] It is widely proven that DESs have similar properties to ionic liquids but have lower production costs, lower toxicity, and higher biodegradability.[37−47] As promising green solvents in analytical chemistry, DESs can be used in sample pretreatment such as extraction, chromatographic separation and analysis, sensing and detection, as well as serving as a reaction medium or functionalization reagent.[48,49] Notably, DESs are widely used as mobile-phase additives in HPLC[50−53] and have been successfully applied to improve the chromatographic separation of targets such as biogenic amines,[54] alkaloids,[55,56] quercetin,[57] and caffeic acid.[58] However, chromatographic separation and analysis involving DESs have rarely been reported for biomolecules such as proteins, peptides, and nucleic acids. In pursuit of both enhanced retention performance and an environmentally friendly mobile phase, the potential of DESs as a mobile-phase additive to separate G4 is worth exploring.

In this work, we systematically investigated the effect of DESs as mobile-phase additives on the retention behavior of different G4s in RP-HPLC by varying both the concentration and the type of DESs. The G4 conformation corresponding to each chromatographic peak was verified by using CD. To further elucidate the role of DESs, surface-enhanced Raman spectroscopy (SERS) was employed to investigate the interaction mode between the DESs and G4 structures. The interactions were visualized via molecular docking, and the underlying retention mechanism was analyzed. This study provides a novel perspective on the application of DESs in G4 chromatographic separation.

EXPERIMENTAL SECTION

Materials and Reagents

The oligonucleotides (listed in Table 1) were all custom-synthesized by Sangon Biotech (Shanghai, China). The ordered oligonucleotides were purified by HPLC, and no further purification was required for experiments. Chromatography grade methanol was purchased from Honeywell (Ulsan, Korea). Tetrabutylammonium bromide (TBAB), KH_2PO_4, K_2HPO_4, glycerol (Gly), sodium citrate, potassium iodine, and 1-butyl-3-methylimidazolium bromide ([BMIm][Br]) were purchased from Aladdin (Shanghai, China). Choline chloride (ChCl), urea, and betaine were purchased from Meryer (Shanghai, China). Malonic acid (MA) and ethylene glycol (EG) were purchased from Macklin (Shanghai, China). Silver nitrate was purchased from Qiangsheng (Jiangsu, China), and magnesium sulfate was purchased from Beyotime Biotechnology (Shanghai, China). The water used was an ultrapure water. All of the other chemicals were of analytical reagent grade unless otherwise noted.

G4 Preparation

Single-stranded oligonucleotides were dissolved in KH_2PO_4−K_2HPO_4 (50 mM, pH 7.0) buffer. The obtained DNA solutions were heated in 95 °C water bath for 10 min and then were cooled to room temperature naturally. Cooled solutions were kept at 4 °C overnight

https://doi.org/10.1021/acs.analchem.5c08145
Anal. Chem. 2026, 98, 16083−16095

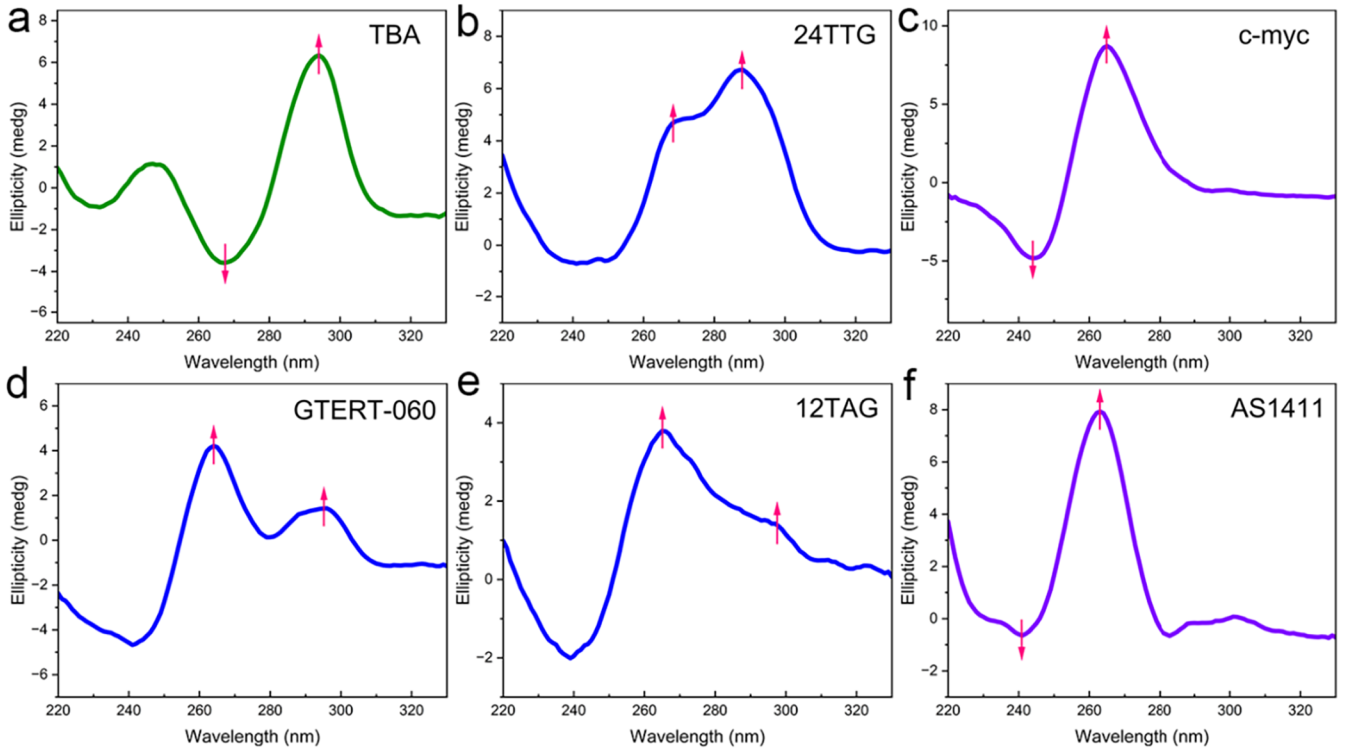

Figure 1. CD spectra of annealed G4-forming sequences in K^+ buffer (50 mM KH_2PO_4–K_2HPO_4, pH 7.0). (a) TBA; (b) 24TTG; (c) c-myc; (d) GTERT-060; (e) 12TAG; (f) AS1411.

and stored at −20 °C before use. Table 1 shows the G4s used in this work.

CD Experiments

CD measurements were performed using a Chirascan digital circular dichroism spectropolarimeter (Applied Photophysics Ltd., England) and a 1 mm path length quartz cuvette. Sampling interval was 0.5 s and slit width was 1 nm. Resulting measurements were the average of three repetitions between 220 and 330 nm at room temperature. CD spectra of baseline and buffer were subtracted from the spectra of sample solutions. The concentration of G4s used for CD measurements was 10 μM. CD melting experiments were performed to observe the attenuation of the signal at 265 nm to record the melting transition. The measured temperature range was 20−95 °C, and the heating rate was 1 °C/min.

Synthesis of DESs

Suitable molar ratios of HBA and HBD were accurately weighed and introduced into a round-bottom flask. The samples were magnetically stirred in an oil bath at 60−100 °C to form a homogeneous and transparent solution. Table 2 provides a detailed list of the DESs used in this work. Both the HBA structures and the synthesized DESs were characterized using infrared spectroscopy, and the results are shown in Figure S1.

SEC Conditions

SEC experiment was performed on LC-20AD (Shimadzu, Kyoto, Japan) with the UV−Vis detector. Separation was accomplished on a TSK_{gel} G2000SW_{XL} column (300 × 7.5 mm i.d., 10 μm). The column temperature was maintained at 30 °C, and the detection wavelength was set at 260 nm. The injection volume was 10 μL. A KH_2PO_4–K_2HPO_4 buffer solution (10 mM, pH 7.0) was used as the mobile phase for isocratic elution at a flow rate of 0.5 mL/min. The final G4 concentration was 50 μM.

RP-HPLC Conditions

RP-HPLC experiments were performed on LC-20AD (Shimadzu, Kyoto, Japan) with the UV−Vis detector. Separation and analysis were accomplished on a Welch Ultimate XB-C18 column (250 × 4.6 mm i.d., 5 μm). The column temperature was maintained at 30 °C, and the detection wavelength was set at 260 nm. The injection volume was 10 μL, and the flow rate was fixed at 1.0 mL/min. The final G4 concentration was 50 μM. Mobile phase A was methanol, and mobile phase B was K^+ buffer and DESs. The gradient mode for mobile phase **1** was 0−15 min, 80% B-55% B; 15−30 min, 55% B-55% B.

Mobile phase B: (A) Basic solution: KH_2PO_4–K_2HPO_4 buffer solution (10 mM, pH 7.0). (B) DES concentration experiments: adding different proportions of DESs to basic solution, respectively; (C) ChCl, TBAB, and [BMIm][Br] concentration experiments: basic solution containing 20 mM ChCl, 2 mM TBAB, and 20 mM [BMIm][Br], respectively.

Surface-Enhanced Raman Spectroscopy (SERS) Conditions

a. Preparation of silver nanoparticles using Lee and Meisel's method:[70] About 36 mg of silver nitrate was weighed and dissolved in 200 mL of purified water. About 4 mL of 1% sodium citrate was slowly added dropwise to the boiling silver nitrate solution, stirred continuously for 40 min until the mixture turned yellowish-green, and stored at 4 °C. Before use, silver sol solution was centrifuged at 5000 rpm for 15 min to remove the supernatant. Characterization of silver nanoparticles: scanning electron microscopy (SEM) images of silver nanoparticles were taken on a Hitachi S-4800 microscope (Hitachi, Tokyo, Japan) connected to a Bruker Quantax energy-dispersive spectrometer (EDS, Bruker, Karlsruhe, German).

b. Fifty microliters of silver sol was mixed with 50 μL of 1 mM potassium iodide solution, incubating at room temperature for 25 min. Then, 50 μL of 25 μM DNA solution and 20 μL of magnesium sulfate solution were added. The color of the solution changed from yellow-green to dark brown.

c. Raman instrument setup: SERS spectra were obtained using a UK laser confocal Raman spectrometer (Renishaw inVia-Reflex). The instrument was automatically calibrated mainly based on the peak value of silicon wafer at 520.5 cm^{-1}. The

https://doi.org/10.1021/acs.analchem.5c08145
Anal. Chem. 2026, 98, 16083−16095

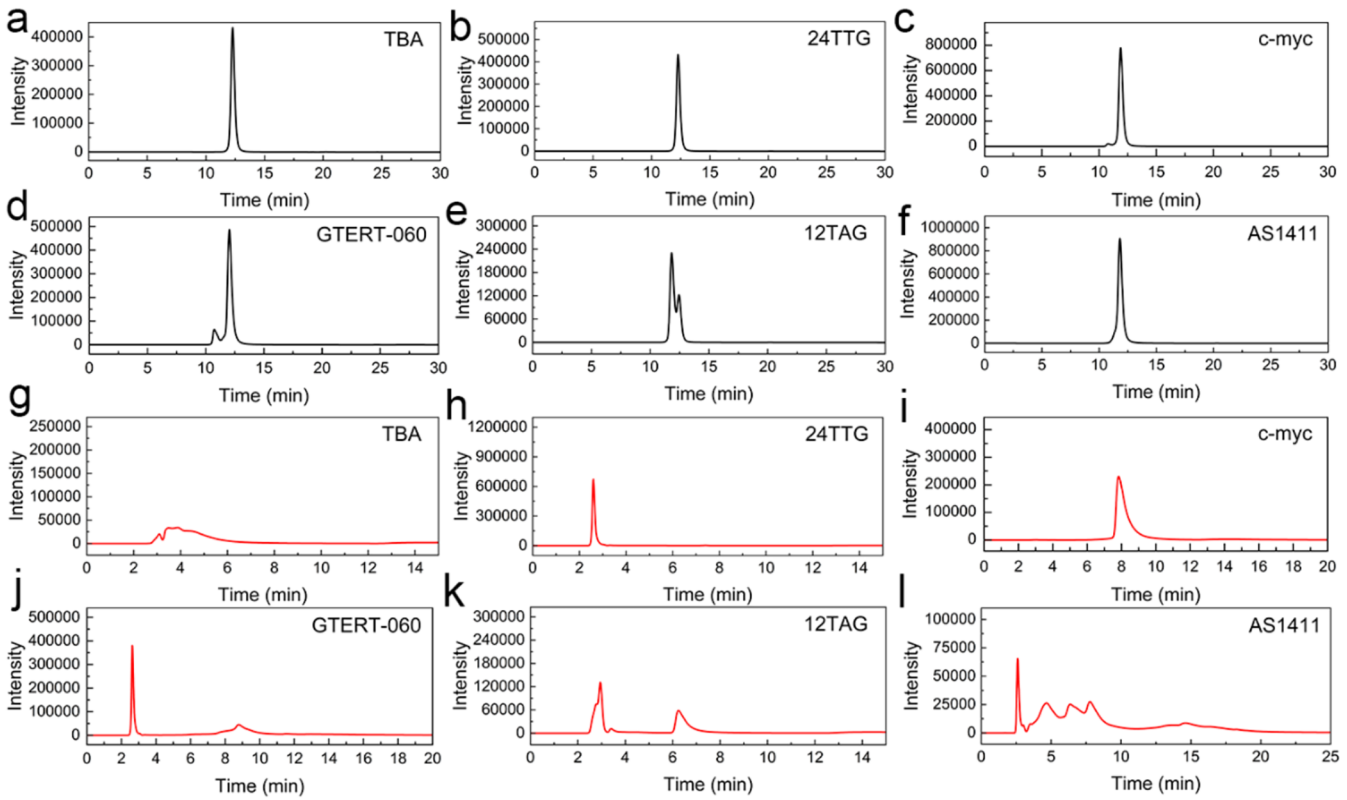

Figure 2. SEC chromatograms of G4s (black line) and RP-HPLC chromatograms of G4s using mobile phase **1** without DES addition (red line). (a) TBA; (b) 24TTG; (c) c-myc; (d) GTERT-060; (e) 12TAG; (f) AS1411; (g) TBA; (h) 24TTG; (i) c-myc; (j) GTERT-060; (k) 12TAG; (l) AS1411.

laser wavelength was 633 nm and the laser energy was 10%; the scan time was 30 s, the accumulation time was one cycle, and the lens was 50 xL. The diameter of the laser spot was 1 μm. Prior to SERS measurements, samples were placed on microscope slides and excited by laser irradiation to obtain SERS spectra. All spectral dates were not additionally processed, and spectrograms were plotted and analyzed using Origin software.

Molecular Docking

The G4 structure was preprocessed in the Protein Preparation Wizard module of Maestro 10.1 software[71] using the OPLS_2005[72] force field. The mol2 files of ChCl and EG 3D structures were downloaded from PubChem (https://pubchem.ncbi.nlm.nih.gov/), and the 3D structures of the ligands were optimized with the OPLS_2005 force field under the LigPrep module. The ligands were docked into each of the three G4 structures by the Glide module in the Maestro program. The receptor lattice box was created with G4 as the centroid, and the default box size was used. Finally, the Glide docking[73,74] method was selected to obtain the docked structures for subsequent analysis.

RESULTS AND DISCUSSION

Confirmation of G4 Structures

Prior to chromatographic experiments, G4 structure formation was confirmed using CD. As shown in Figure 1, all of the nucleic acid sequences in this study were able to form G4 structures after annealing. TBA formed an antiparallel structure with a characteristic positive peak around 295 nm and a negative peak at 265 nm.[60] 24TTG, GTERT-060, and 12TAG all showed two positive peaks near 265 and 295 nm, representing the formation of hybrid or mixed G4s. According to the literature, 24TTG formed a (3 + 1) hybrid G4 topology,[63] GTERT-060,[67] and 12TAG[68] folded into multiple structures. AS1411 and c-myc were shown to form parallel structures in CD spectra with a positive peak near 265 nm and a negative peak near 240 nm. However, according to reports,[69] AS1411 could form at least eight different structures after annealing in K^+ buffer, exhibiting highly diverse structural morphologies and mainly based on parallel structures.

Comparison of G4 Separation by SEC and RP-HPLC

K^+ was the main component of the annealing solution, and phosphates were common buffer solutions in liquid chromatography. We chose the K_2HPO_4–KH_2PO_4 buffer solution as the mobile phase. For most of the experiments on the structures, interactions, and applications of G4s were carried out under neutral conditions, so the mobile-phase pH was adjusted to 7.0. Previous studies showed that gradient elution was an effective method for separating different G4 conformations in RP-HPLC.[32,33] Gradient elution was used for all RP-HPLC in this experiment.

First, a comparison of the separation efficiency between SEC and RP-HPLC was carried out in a mobile phase without DESs. The results in Figure 2a–f showed that SEC was favorable for analyzing single-conformation G4s, such as TBA, 24TTG, and c-myc. However, for G4s with multiconformations, such as GTERT-060, 12TAG, and AS1411, SEC was ineffective in separating them. In particular, for AS1411, only one peak could be detected. Compared with SEC, RP-HPLC was more efficient for separating different conformations of G4s, which has been proven in our previous work.[32] However, Figure 2g–l shows that the studied G4s in this work had poor separation and peak shapes under the commonly used RP-HPLC method. Previous research has indicated that DESs are capable of maintaining G4 structures.[75,76] Therefore, prior to

https://doi.org/10.1021/acs.analchem.5c08145
Anal. Chem. 2026, 98, 16083−16095

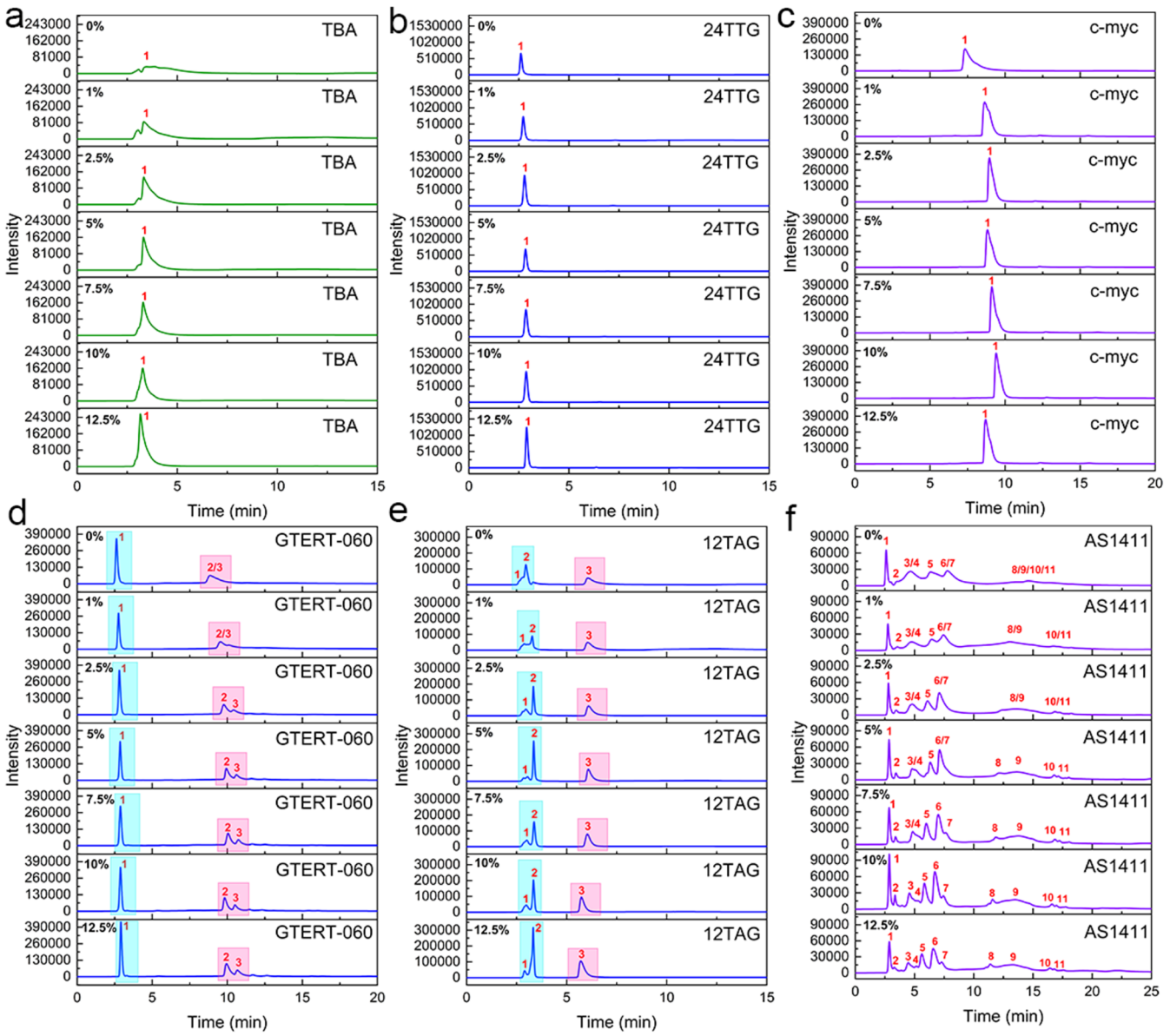

Figure 3. RP-HPLC chromatograms of G4s at different concentrations of DES1 (ChCl:EG = 1:3). (a) TBA; (b) 24TTG; (c) c-myc; (d) GTERT-060; (e) 12TAG; (f) AS1411. RP-HPLC chromatograms were obtained using mobile phase **1** with DES addition. Mobile phase A was methanol and mobile phase B was KH_2PO_4–K_2HPO_4 buffer solution (10 mM, pH 7.0) with 0, 1, 2.5, 5, 7.5, 10, 12.5% (v/v) DES1, respectively.

adding DES to the chromatographic mobile phase, CD analysis was performed to study the effect of DESs on the G4 structures. As illustrated in Figure S2a–l, except for DES7, all other DESs could maintain the G4 structures.

Effect of ChCl and EG-Based DESs on G4 Retention Behavior

ChCl- and EG-based DESs are among the most common DESs. Compared to other DESs, they have lower viscosity, making them a better choice for use as mobile-phase additives. As shown in Figure 3a, in the absence of DES, the TBA peak was susceptible to split and the peak shape underwent severe broadening. When DES1 (ChCl:EG = 1:3) was added to the mobile phase, the splitting of the TBA peak was gradually weakened and the peak shape improved with increasing DES1 concentration. As shown in Figure 3b,c, the retention times of 24TTG and c-myc increased with the addition of DES1. Interestingly, when more than 10% of DES1 was added, the retention time of c-myc was shortened. That is, when excessive DES1 was introduced, DES1 attached to the C18 surface through electrostatic interaction and competed with G4 so that weakening G4 retention.

Notably, the retention time of c-myc was obviously longer than those of TBA and 24TTG. Studies have demonstrated that hydrophobic base stacking plays an apparent role in the stability of the DNA double helix.[77] Similarly, in G4 structures, the G-quartets formed by guanine stacking were the main hydrophobic sites of G4s.[33] For parallel c-myc, due to the loop regions being located on the outside of G-quartet layers, the steric hindrance of the terminal G-quartets is small, which facilitates stronger hydrophobic interactions with the C18 stationary phase, resulting in longer retention time. Conversely, in the nonparallel TBA and 24TTG, the loop regions are located above or below the G-quartet layers, resulting in significant steric hindrance to the terminal G-quartets. This spatial constraint impedes effective hydrophobic interactions

https://doi.org/10.1021/acs.analchem.5c08145
Anal. Chem. 2026, 98, 16083−16095

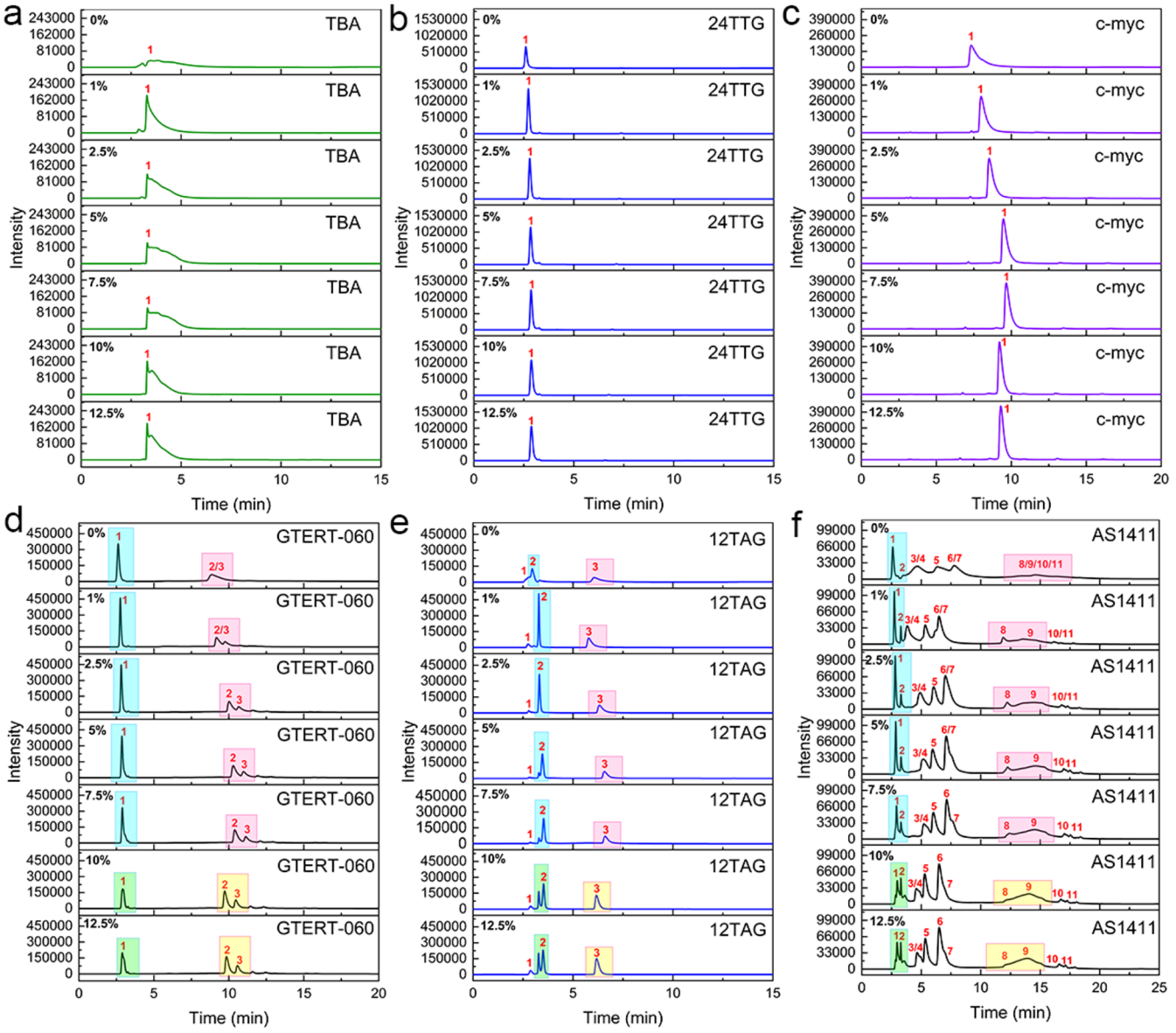

Figure 4. RP-HPLC chromatograms of G4s at different concentrations of DES5 (ChCl:Urea = 1:2). (a) TBA; (b) 24TTG; (c) c-myc; (d) GTERT-060; (e) 12TAG; (f) AS1411. RP-HPLC chromatograms were obtained using mobile phase **1** with DES addition. Mobile phase A was methanol and mobile phase B was KH_2PO_4–K_2HPO_4 buffer solution (10 mM, pH 7.0) with 0, 1, 2.5, 5, 7.5, 10, 12.5% (v/v) DES5, respectively.

between the G-quartets and the C18 surface, thereby leading to shorter retention.

For GTERT-060 and 12TAG with multiple structures, as shown in Figure 3d,e, their chromatographic peaks could be divided into two distinct parts. The less retained species (Part 1, highlighted by the blue rectangle in Figure 3d,e) exhibited a retention behavior similar to that of TBA and 24TTG, suggesting they may adopt nonparallel G4 topologies. The more strongly retained species (Part 2, pink rectangle in Figure 3d,e) exhibited a retention trend similar to that of c-myc, implying that they may possess structural characteristics similar to parallel G4. Compared with the chromatograms obtained in the absence of DES1, the retention times of both GTERT-060 and 12TAG initially increased and then decreased with increasing concentrations of DES1. Furthermore, chromatographic resolution was also significantly improved. In the case of AS1411, which adopts more complex structures, a noticeable improvement in chromatographic separation was observed as the concentration of DES1 increased to 7.5%. As shown in Figure 3f, a total of 11 peaks were clearly observed. These results demonstrated that the addition of DES1 to the mobile phase effectively optimized the RP-HPLC retention behavior of G4s by improving both peak shape and separation resolution and enhanced retention time partly.

To identify the specific G4 structure corresponding to each chromatographic peak, we analyzed the peak effluent using CD. The detailed information is shown in the Supporting Information (confirmation of G4 chromatographic peak conformation). It showed that the TBA peak displayed an antiparallel topology (Figure S3a). The 24TTG peak exhibited a hybrid structure (Figure S3b). c-Myc showed a parallel structure (Figure S3c). These results confirmed that these G4 structures remained intact during RP-HPLC analysis.

In Figure S3d–f, the CD spectra corresponded to three chromatographic peaks of GTERT-060. Peak 1 displayed a hybrid structure. Both peaks 2 and 3 demonstrated parallel G4

https://doi.org/10.1021/acs.analchem.5c08145
Anal. Chem. 2026, 98, 16083−16095

structures. The CD profiles of 12TAG are depicted in Figure S3g−i. Peak 1 lacked characteristic CD signals, implying that it might correspond to a single-stranded form. Peak 2 showed a broad and elevated absorption spanning 265−295 nm, suggesting a mixture of structures. Peak 3 presented a parallel conformation.

Figure S3j−n shows the CD spectra for AS1411. Due to the weak intensity of peaks 2, 4, 7, 8, 10, and 11, these fractions were pooled with adjacent peaks for analysis. The combined peaks 1 + 2 showed no discernible CD signature, while peaks 3 + 4, peak 5, peaks 6 + 7, and peaks 8 + 9 + 10 + 11 all represented parallel structures. This indicates that AS1411 predominantly adopts a parallel conformation. The CD findings were in agreement with our speculation about the peak structures discussed in the preceding discussion. Moreover, these data demonstrated that the RP-HPLC method with DES1 as the mobile-phase additive had the ability to effectively separate different G4 conformations while maintaining the G4 structures.

The identification results of each peak conformation by CD described above provided direct confirmation of our earlier speculation regarding the peak conformation within Part 1 and Part 2 of GTERT-060 and 12TAG, based on the observed changes in retention behavior.

Considering that DESs synthesized at different molar ratios and temperatures exhibit distinct physicochemical properties (such as the number of hydrogen bonds and viscosity), we then prepared a series of DESs and investigated their effects on retention behavior of G4s. DES2, also synthesized from ChCl and EG but at a molar ratio of 1:2 (same temperature: 80 °C), exhibited a similar influence on G4 retention behavior as DES1 when used as a mobile-phase additive, though it induced a slightly greater increased in G4 retention time (Figure S4). DES3 and DES4 were prepared at the same molar ratio of ChCl to EG (1:3) but at different temperatures (60 and 100 °C, respectively). As shown in Figure S5, both displayed effects on G4 retention behavior comparable to DES1 at 5% additive concentration. These findings indicated that variations in the synthesis molar ratio and temperature of DESs had only a minor influence on the chromatographic retention behavior of G4s.

Effect of ChCl and Urea-Based DESs on G4 Retention Behavior

It has been reported that G4 can remain stable in ChCl and urea-based DESs, with the parallel structure emerging as the preferred conformation.[76] DES5 (ChCl:urea = 1:2) was used as a mobile-phase additive, and the results are shown in Figure 4. Conversely, DES5 did not improve the peak shape of TBA, as shown in Figure 4a. For 24TTG and c-myc, the retention tendency was similar to that in Figure 4b,c. The retention time of G4s increased when the volumetric ratio of DES5 in the mobile phase increased, but this effect was diminished when it exceeded 7.5%. This phenomenon occurred because, when too much DES5 was added, DES5 competed with G4s for the C18 surface, reducing the retention of G4s. For G4s with multiple conformations, DES5 induced different effects on their chromatographic retention behaviors. Unlike DES1, when DES5 was added at concentrations up to 10%, the intensity of peak 1 in GTERT-060 decreased, while the intensity of peaks 2 and 3 increased (Figure 4d). This indicated a partial structural transition from nonparallel G4 to parallel G4 conformations within GTERT-060. A similar conformational shift was observed for 12TAG, as shown in Figure 4e. When the addition of DES5 was up to 5%, more shifts of peak 2 occurred. When the concentration of DES5 was increased to 10%, the intensity of peak 3 increased, indicating a rise in the proportion of parallel G4 structures. The conformational shift phenomenon also occurred with AS1411, as shown in Figure 4f. Peaks 1 and 2 appeared to be cleaved when the volume ratio of DES5 reached 10%. At the same time, peak 8 weakened, and peak 9 increased in intensity. Overall, DES5 improved the chromatographic separation of G4s with multiple conformations at low concentration; however, it induced structural transformations in G4 structures at higher concentrations. Moreover, because of its high viscosity, the long-term use of DES5 in liquid chromatography was not recommended.

Effect of ChCl and Gly-Based DESs on G4 Retention Behavior

Upon introduction of DES6 into the mobile phase in the same way, it was found that retention and peak shape of G4s differ markedly from those obtained with DES1 to DES5, as shown in Figure S6. We speculated that G4 structures were disrupted under these conditions. However, CD spectroscopy (Figure S2g−l) indicated that DES6 itself did not disrupt the G4 structures. To clarify the distinct retention behavior of G4s in DES6, we considered the physicochemical properties of DES6: its HBD is glycerol, which exhibits a high viscosity. As a result, when mobile phase B (containing DES6) was mixed with mobile phase A (methanol) online, high viscosity impeded sufficient mixing of the two phases. This resulted in considerable fluctuations in K^+ concentration during the gradient process, thereby destabilizing the G4 structures and ultimately causing the observed chromatographic retention behavior.

To overcome this issue, we implemented a premixed strategy for the mobile phases to facilitate rapid K^+ concentration equilibration during gradient. The compositions were set as follows: mobile phase A (80% methanol, 20% K^+ buffer containing DES6) and mobile phase B (20% methanol, 80% K^+ buffer containing DES6). Using the gradient elution program of 0−15 min from 100 to 60% B, followed by a 15 min hold at 60% B (mobile phase **2**), we achieved obviously faster mixing and K^+ equilibrium compared with the nonpremixed system (mobile phase **1**). Reinvestigation of G4s with DES6 in mobile phase **2** revealed a retention behavior similar to that with DES1 (Figure S7). However, control experiments using DES1 at concentrations of 1, 5, and 10% showed nearly identical G4 retention behavior in mobile phase **2** (Figure S8) as that in mobile phase **1** (Figure 3). This further indicated that the G4 retention anomaly with DES6 in mobile phase **1** was conclusively attributed to the high viscosity of DES6 impeding mixing. In addition, it should be noted that glycerol-induced high viscosity can cause high column pressure and baseline instability, rendering DES6 unsuitable for long-time testing. Nonetheless, these findings identified obvious K^+ concentration fluctuations as a cause of "structural collapse" in the analysis of G4s, a critical methodological consideration.

Effect of Other DESs on G4 Retention Behavior

We also investigated the effects of DES7 (ChCl-MA) and DES8 (betaine-EG) on G4 retention behavior, as summarized in Figure S9. The results indicated that the acidity of DES7 destroyed G4 structures (Figure S2g−l) and adversely affected the corresponding chromatographic peaks. Compared with DES1, DES8 improved the peak shape of the TBA. However, it

https://doi.org/10.1021/acs.analchem.5c08145
Anal. Chem. 2026, 98, 16083−16095

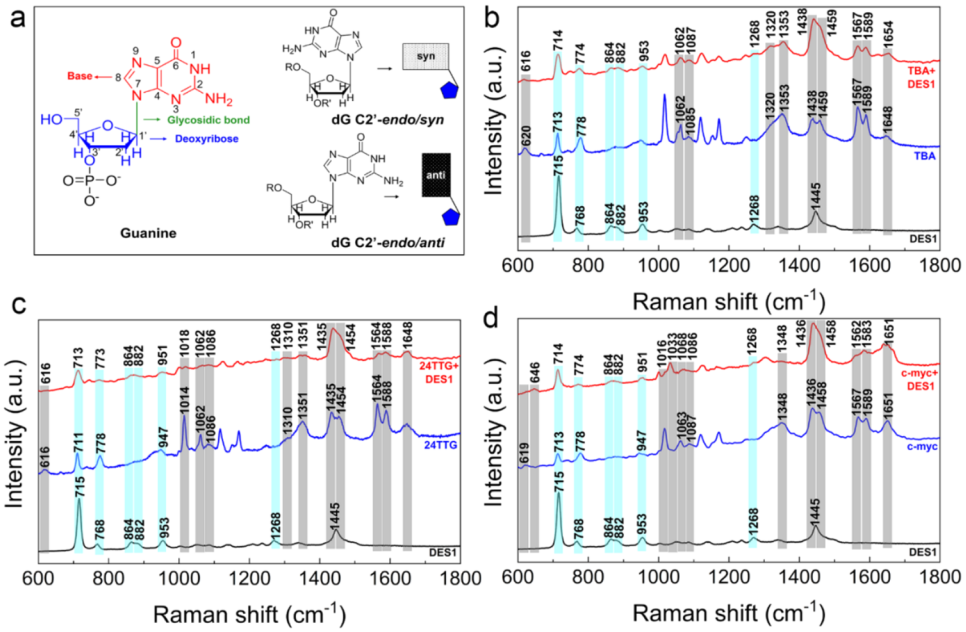

Figure 5. Impact of DES1 on the SERS signal of G4s. (a) Guanine nucleotide structure and *syn*/*anti* glycosidic angular conformations of dG C2′-*endo*. (b−d) SERS spectra of DES1, G4, and G4+DES1 obtained by using AgIMgNPs as substrate. DES1 (black), G4 (blue), and G4+5% DES1 (red).

showed poor separation efficiency for G4s involving multiple conformations. Notably, the use of DES8 in the mobile phase shortened G4 retention. This can be attributed to the amphoteric ionic nature of betaine, which, unlike ChCl, carries a negative charge that influences G4 retention.

In summary, among the tested DESs, DES1 proved to be the most suitable mobile-phase modifier due to its low viscosity, minimal disruption of G4 structures, and effective chromatographic separation performance.

Selection of Column Temperature for G4 Separation

When high concentrations of DESs were used as mobile-phase additives, the column pressure was always high, which was detrimental to column efficiency. Although increasing column temperature is a known strategy to reduce backpressure and could theoretically benefit the analysis, CD melting experiments revealed that some G4s began to unfold at temperatures exceeding 30 °C, as corroborated by the data presented in Figure S10. Therefore, to preserve the G4 structure during separation, it is best to maintain the column temperature below or equal to 30 °C.

Exploring Roles and Functions of DES Components

To systematically evaluate whether G4 retention behavior was influenced more by HBD or HBA, we employed partial DESs and individual HBAs as mobile-phase additives for comparative analysis. DES1, DES9, and DES10, which share the same HBD (ethylene glycol, EG) but differ in HBA, were selected. To ensure the reasonableness of the G4 retention time, we selected appropriate concentrations of each HBA and DES, respectively. Results (Figure S11) showed that the effect of DES1 on G4 retention behavior was similar to ChCl. DES9 mirrored the effect of TBAB, and DES10 showed an effect comparable to that of [BMIm][Br]. These findings suggested that the HBA component was the primary factor in DESs affecting G4 retention behavior.

Furthermore, the effect of HBDs was evaluated by the comparison of DES1 and DES5, which share the same HBA (ChCl) but differ in their HBDs. When used as mobile-phase additives, these two DESs induced distinct G4 retention behavior, as illustrated in Figures 3 and 4. This indicated that HBDs also contributed to G4 retention but their effect was less pronounced than that of HBAs.

SERS Reveals the Interaction Mode between DES1 and G4s

SERS, which provides detailed molecular vibration information, has proven effective for G4 conformation analysis.[22,78−80] To elucidate the mechanism of DES1, we designed a systematic study using three representative G4 sequences, each containing only a single conformation: the antiparallel TBA, the hybrid-type 24TTG, and the parallel c-myc. This selection comprehensively covered the major G4 topological families, enabling a comparative investigation of how DES1 interacted with distinct G4 structures.

In this study, AgNPs were used as the substrate, I^- was added to remove interference, and Mg^{2+} was used to induce aggregation of silver nanoparticles to amplify the Raman signal.[81,82] As shown in Figure S12, SEM revealed that the silver nanoparticles aggregated after the addition of Mg^{2+}. Using TBA as an example (Figure S13), in the absence of Mg^{2+}, the Raman signals were weak even when the laser energy of the instrument was amplified by 10 times. In contrast, after adding Mg^{2+}, strong signals were readily obtained at a standard laser energy. Furthermore, we compared the SERS spectra of three G4 sequences dissolved in water versus those in K^+ solution (Figure S14). New spectral bands emerged after G4 formation (corresponding to G4s in K^+ solution), along with the changes in the intensity and position of certain bands, and the detailed information is described in Text S1. The chemical structure of guanine nucleotide[83] is shown in Figure 5a. The major bands in the spectra of single-stranded DNAs and G4s were assigned referring to the literature and are summarized in Tables S1 and S2.

https://doi.org/10.1021/acs.analchem.5c08145
Anal. Chem. 2026, 98, 16083−16095

We further compared the SERS spectra of G4s before and after adding DES1. The SERS spectra of TBA, DES1 and TBA-DES1 complex (Figure 5b) showed that after binding with DES1, the peak at 620 cm^{-1} (dT-loop) shifted, suggesting that DES1 interacted with dT in the loop. The intensity of deoxyribose (1062 cm^{-1}) changed and the peak signal of phosphate backbone (1087 cm^{-1}) shifted, indicating DES1 interacted with the deoxyribose phosphate backbone of TBA. In the SERS spectrum of TBA alone, peaks representing dG C2′-*endo*/*syn* (1320 cm^{-1}) and dG C2′-*endo*/*anti* (1353 cm^{-1}) were observed. After binding with DES1, both peak shapes changed obviously, demonstrating that DES1 interacted with *syn*/*anti* guanine in G4s, with a stronger interaction toward *syn*-guanine. Additionally, the signals at 1438 cm^{-1} (deoxyribosyl C5′-H_2) and 1459 cm^{-1} (dG N7 (strong Hoogsteen H-bond)) were enhanced, with a more pronounced shoulder at 1459 cm^{-1}. The relative intensities of the signals at 1567 cm^{-1} (dG δNH (N2H interbase H-bond)) and 1589 cm^{-1} (dG δNH (N1H interbase H-bond)) were altered, indicating that DES1 interacted with dG of G-tetrad planes and thereby affecting the signal intensity. The band shift at 1648 cm^{-1} (dT) also indicated the interaction between DES1 and dT. In addition, peak positions of 714, 774, 864, 882, 953, 1268, and 1445 cm^{-1} originating from DES1 itself were observed in the SERS spectra of TBA-DES1. Among them, peaks overlapping with those of TBA alone showed increased peak intensity in the complex. For 24TTG and c-myc, the SERS results were similar to those of TBA (Figure 5c,d), and the detailed information is provided in Text S2.

Taken together, the above SERS results clearly indicated that specific interactions occurred between DES1 and G4s. Notably, the binding sites of DES1 were mainly found in the groove region and phosphate backbone, regardless of the G4 conformation.

Molecular Docking Visualized the Interaction Mode between DES1 and G4s

We performed molecular docking on ChCl and G4 as well as EG and G4, separately. Notably, EG did not show significant binding to any specific site of the G4s (Figure S15). In contrast, ChCl successfully docked with the G4s, primarily within the groove region, as depicted in Figure S16.

Detailed analysis revealed distinct interaction profiles for each G4. In the case of TBA, ChCl formed hydrogen bonds with dT9 in the loop region and with *syn*-dG10 in the G-tetrad planes. Additional interactions were observed with dG11, dG14, and dG15 within the G-tetrad planes (Figure S16a−c). For 24TTG, ChCl formed a hydrogen bond with the terminal dT1. Furthermore, the quaternary ammonium group of ChCl engaged in cation-π interactions with *anti*-dG5 in the G-tetrad planes. Additional interactions involved dT6 and dT7 in the loop, as well as dG3, dG4, and dG9 in the G-tetrad planes (Figure S16d−f). Regarding the c-myc, docking results showed that ChCl formed hydrogen bonds with *anti*-dG9 and *anti*-dG13 and participated in cation-π interactions with the conjugated systems of the G-tetrad planes. Besides, an interaction with dT11 in the loop was also identified (Figure S16g−i). Additionally, electrostatic interactions existed between $[ChCl]^+$ and the G4 phosphate backbone. Taking c-myc as an example, ChCl occupied the pocket formed by dG9, dG10, dT11, dA12, dG13, dG14, and dG15. Within this pocket, dG9 and dG13 brought the G4 phosphate backbone closer to the $[ChCl]^+$ ion by interacting with the hydroxyl group, thereby facilitating electrostatic attraction between the anionic backbone and the cationic choline moiety.

Collectively, the molecular docking results were strongly consistent with the findings from the SERS assay, further corroborating the specific binding mode of ChCl to various G4s.

Mechanism Elucidation of Retention Behavior

In RP-HPLC, the retention of G4s is primarily governed by hydrophobic interactions between the G-tetrad planes and the C18 stationary phase. To confirm the dominant contribution of hydrophobic interactions, we further compared the retention behaviors of G4s under identical experimental conditions using C8 and C4 columns with equivalent specifications. As shown in Figure S17, under the same elution protocol, G4s exhibited the shortest retention time and the poorest resolution on the C4 column. While the C8 column provided partial separation, it did not achieve the same separation efficiency as the C18 column. These results clearly demonstrated that hydrophobic interactions play a critical role in the retention of G4s in RP-HPLC.

To assess the stability of the C18 column under the employed conditions, its performance was monitored with 5% DES1 as the mobile-phase additive. As shown in Figure S18a−f, the retention time, peak shape, and resolution of G4s after long-term use were basically consistent with those observed during initial use. This consistency suggests that the interaction between DES and the C18 stationary phase is predominantly based on reversible physical adsorption rather than permanent chemical modification or stationary phase leaching from the column. To maximize the column lifetime, routine rinsing with the mixture of water and methanol in different proportions after analysis is recommended to ensure complete removal of any residual components.

The good separation, peak shape, and the changed retention observed for G4s with the addition of DES1 in the mobile phase on C18 column could be attributed to the following reasons: (a) **Enhanced hydrophobicity**. Specifically, ChCl engages with G4s via groove binding, supported by hydrogen bonding, cation-π, and electrostatic interactions. Besides, ChCl neutralizes the deoxyribose phosphate backbone negative charges. These interactions enhance the hydrophobicity of G4s, enabling them to approach the C18 surface more closely, improving their retention. (b) **Masking silanol hydroxyl effect**. The pK_a value of silanol group was about 4.5−4.7. At pH 7.0, residual silanol groups on the C18 stationary phase are predominantly deprotonated, forming negatively charged silanolate ($Si-O^-$) sites. These anionic sites can engage in undesirable electrostatic interactions with protonated basic moieties in G4 molecules, often leading to pronounced peak tailing and compromised resolution. Upon the addition of DES1, the choline cation ($[ChCl]^+$) can electrostatically associate with the exposed silanolate groups, thereby effectively shielding or passivating these active sites. This masking effect mitigates the unwanted secondary interactions, resulting in improved peak symmetry and enhanced separation efficiency for G4 structures.

In summary, the retention of G4s in reversed-phase liquid chromatography is predominantly governed by hydrophobic interactions. The introduction of DES1 changed the G4 retention, improved the peak shape, and increased the separation efficiency. The mechanism is illustrated in Figure 6.

https://doi.org/10.1021/acs.analchem.5c08145
Anal. Chem. 2026, 98, 16083−16095

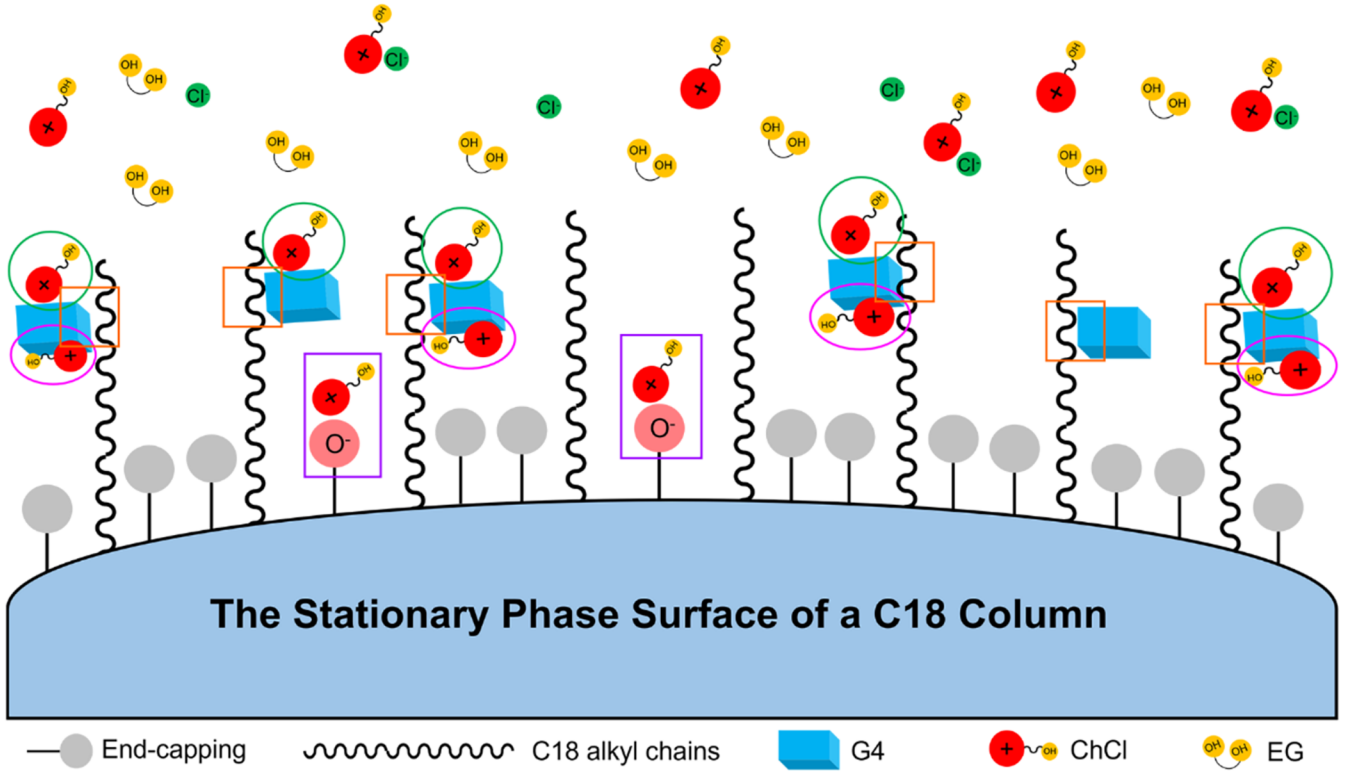

Figure 6. Interaction mechanisms between DES1, G4s, and the stationary phase surface of the silica-based C18 column. The purple rectangles represent the electrostatic attraction between $[ChCl]^+$ and anionic silanol groups. The orange rectangles represent the hydrophobic interaction between C18 alkyl chains and G4s. The green circle represent the electrostatic interaction between $[ChCl]^+$ and negatively charged deoxyribose phosphate backbones of G4s. The pink ovals represent the groove bonding between ChCl and G4s, supported by hydrogen bonding, cation-π, and electrostatic interactions.

CONCLUSIONS

RP-HPLC is an effective tool for analyzing complex biological systems and has great potential for elucidating the G4 polymorphism. In this article, DESs were introduced as mobile-phase additives to comprehensively investigate how they amended the retention behaviors of various G4s in RP-HPLC. The results revealed that DES1 apparently enhanced the chromatographic separation, improved peak shapes, and changed G4 retention. Among the studied DESs, the impact of different DESs on G4s varied. This reflected the diversity in the interactions between DESs and G4s. Both HBD and HBA contributed to G4 retention with HBA playing a dominant role. However, G4 retention was primarily affected by the level of the DES content. The binding sites of DES1 and different structural G4s were investigated in detail by SERS and molecular docking. The results showed that G4s and DES1 were combined at the groove position and phosphate backbone. Furthermore, CD was employed to unambiguously assign G4 conformations to distinct chromatographic peaks, confirming that parallel G4s exhibit greater hydrophobicity than nonparallel G4s. Notably, this work presents the first application of DESs for enhancing G4 separation in RP-HPLC and the first implementation of SERS to probe DES-G4 interactions and their underlying mechanisms. These findings collectively establish DESs as environmentally friendly and promising modifiers for improving the separation of structurally complex biomolecules, such as G4s, in RP-HPLC. Beyond this methodological advance, the strategy also offers a prospect for isolation of homogeneous conformations, which facilitates more precise structure–activity relationship analyses and enables conformation-specific ligand design and development. The approach may further extend to other conformationally heterogeneous nucleic acid structures such as i-motifs. Overall, this work introduces a sustainable separation strategy, opens new avenues for exploring structure–function relationships of G4s, and holds promise for wider applications.

ASSOCIATED CONTENT

Supporting Information

The Supporting Information is available free of charge at https://pubs.acs.org/doi/10.1021/acs.analchem.5c08145.

Infrared spectra, CD spectra, RP-HPLC chromatograms, CD melting curves, SEM images, SERS spectra, SERS spectra description, and SERS spectral assignment (PDF)

AUTHOR INFORMATION

Corresponding Authors

Jun-qin Qiao − *State Key Laboratory of Analytical Chemistry for Life Science, School of Chemistry and Centre for Shared Scientific Research Facilities, Nanjing University, Nanjing 210023, China*; Phone: +86-25-83686075; Email: qiaojunqin@nju.edu.cn; Fax: +86-25-83325180

Hong-zhen Lian − *State Key Laboratory of Analytical Chemistry for Life Science, School of Chemistry and Centre for Shared Scientific Research Facilities, Nanjing University, Nanjing 210023, China*; orcid.org/0000-0003-1942-9248; Email: hzlian@nju.edu.cn

https://doi.org/10.1021/acs.analchem.5c08145
Anal. Chem. 2026, 98, 16083−16095

Authors

Lu-yan An − *State Key Laboratory of Analytical Chemistry for Life Science, School of Chemistry and Centre for Shared Scientific Research Facilities, Nanjing University, Nanjing 210023, China*

Long-yu Zhu − *State Key Laboratory of Analytical Chemistry for Life Science, School of Chemistry and Centre for Shared Scientific Research Facilities, Nanjing University, Nanjing 210023, China*

Min Zhu − *State Key Laboratory of Analytical Chemistry for Life Science, School of Chemistry and Centre for Shared Scientific Research Facilities, Nanjing University, Nanjing 210023, China*

Weijuan Zheng − *State Key Laboratory of Pharmaceutical Biotechnology, School of Life Sciences, Nanjing University, Nanjing 210023, China*

Xiaojun Yao − *Centre for Artificial Intelligence Driven Drug Discovery, Faculty of Applied Sciences, Macao Polytechnic University, Macao 999078, China;* orcid.org/0000-0001-9958-8438

Complete contact information is available at: https://pubs.acs.org/10.1021/acs.analchem.5c08145

Author Contributions

L.-y.A.: Data curation, formal analysis, investigation, methodology, validation, visualization, writing—original draft. L.-y.Z.: Visualization, investigation, formal analysis, data curation. M.Z.: Visualization, methodology, data curation. J.-q.Q.: Formal analysis, funding acquisition, resources, supervision, writing—review and editing. W.Z.: Conceptualization, supervision. X.Y.: Software. H.-z.L.: Conceptualization, funding acquisition, resources, supervision, writing—review and editing.

Notes

The authors declare no competing financial interest.

■ ACKNOWLEDGMENTS

This work was supported by the National Natural Science Foundation of China (Nos. 22304075, 21577057, 91643105, 21874065, and 22176085) and the National Key R&D Program of China (No. 2021YFF0600800).

■ REFERENCES

(1) Mergny, J.-L.; Sen, D. DNA Quadruple Helices in Nanotechnology. *Chem. Rev.* **2019**, *119* (10), 6290−6325.

(2) Gros, J.; Rosu, F.; Amrane, S.; De Cian, A.; Gabelica, V.; Lacroix, L.; Mergny, J.-L. Guanines are a quartet's best friend: impact of base substitutions on the kinetics and stability of tetramolecular quadruplexes. *Nucleic Acids Res.* **2007**, *35* (9), 3064−3075.

(3) Kosiol, N.; Juranek, S.; Brossart, P.; Heine, A.; Paeschke, K. G-quadruplexes: a promising target for cancer therapy. *Mol. Cancer* **2021**, *20* (1), No. 40.

(4) Nishio, M.; Tsukakoshi, K.; Ikebukuro, K. G-quadruplex: Flexible conformational changes by cations, pH, crowding and its applications to biosensing. *Biosens. Bioelectronics* **2021**, *178*, No. 113030.

(5) Ferreira, R.; Marchand, A.; Gabelica, V. Mass spectrometry and ion mobility spectrometry of G-quadruplexes. A study of solvent effects on dimer formation and structural transitions in the telomeric DNA sequence d(TAGGGTTAGGGT). *Methods* **2012**, *57* (1), 56−63.

(6) Zhou, J.; Tateishi-Karimata, H.; Mergny, J.-L.; Cheng, M.; Feng, Z.; Miyoshi, D.; Sugimoto, N.; Li, C. Reevaluation of the stability of G-quadruplex structures under crowding conditions. *Biochimie* **2016**, *121*, 204−208.

(7) Vorlíčková, M.; Bednářová, K.; Kypr, J. Ethanol is a better inducer of DNA guanine tetraplexes than potassium cations. *Biopolymers* **2006**, *82* (3), 253−260.

(8) Phan, A. T. Human telomeric G-quadruplex: structures of DNA and RNA sequences. *FEBS J.* **2010**, *277* (5), 1107−1117.

(9) Burge, S.; Parkinson, G. N.; Hazel, P.; Todd, A. K.; Neidle, S. Quadruplex DNA: sequence, topology and structure. *Nucleic Acids Res.* **2006**, *34* (19), 5402−5415.

(10) Bhattacharyya, D.; Mirihana Arachchilage, G.; Basu, S. Metal cations in G-quadruplex folding and stability. *Front. Chem.* **2016**, *4*, 1−14.

(11) Gray, R. D.; Chaires, J. B. Linkage of cation binding and folding in human telomeric quadruplex DNA. *Biophys. Chem.* **2011**, *159* (1), 205−209.

(12) Chaudhary, S.; Kumar, M.; Kaushik, M. Interface of G-quadruplex with both stabilizing and destabilizing ligands for targeting various diseases. *Int. J. Biol. Macromol.* **2022**, *219* (31), 414−427.

(13) Spiegel, J.; Adhikari, S.; Balasubramanian, S. The structure and function of DNA G-quadruplexes. *Trends Chem.* **2020**, *2* (2), 123−136.

(14) Carvalho, J.; Mergny, J.-L.; Salgado, G. F.; Queiroz, J. A.; Cruz, C. G-quadruplex, friend or foe: the role of the g-quartet in anticancer strategies. *Trends Mol. Med.* **2020**, *26* (9), 848−861.

(15) Wang, E.; Thombre, R.; Shah, Y.; Latanich, R.; Wang, J. G-Quadruplexes as pathogenic drivers in neurodegenerative disorders. *Nucleic Acids Res.* **2021**, *49* (9), 4816−4830.

(16) Dong, J.; O'Hagan, M. P.; Willner, I. Switchable and dynamic G-quadruplexes and their applications. *Chem. Soc. Rev.* **2022**, *51* (17), 7631−7661.

(17) Zhou, J.; Amrane, S.; Rosu, F.; Salgado, G. F.; Bian, Y.; Tateishi-Karimata, H.; Largy, E.; Korkut, D. N.; Bourdoncle, A.; Miyoshi, D.; Zhang, J.; Ju, H.; Wang, W.; Sugimoto, N.; Gabelica, V.; Mergny, J.-L. Unexpected position-dependent effects of ribose g-quartets in G-quadruplexes. *J. Am. Chem. Soc.* **2017**, *139* (23), 7768−7779.

(18) Winnerdy, F. R.; Bakalar, B.; Maity, A.; Vandana, J. J.; Mechulam, Y.; Schmitt, E.; Phan, A. T. NMR solution and X-ray crystal structures of a DNA molecule containing both right- and left-handed parallel-stranded G-quadruplexes. *Nucleic Acids Res.* **2019**, *47* (15), 8272−8281.

(19) Ambrus, A.; Chen, D.; Dai, J.; Bialis, T.; Jones, R. A.; Yang, D. Human telomeric sequence forms a hybrid-type intramolecular G-quadruplex structure with mixed parallel/antiparallel strands in potassium solution. *Nucleic Acids Res.* **2006**, *34* (9), 2723−2735.

(20) Wang, J.; Qiao, J.; Zheng, W.; Lian, H. Study on the interaction of a peptide targeting specific G-quadruplex structures based on chromatographic retention behavior. *Int. J. Mol. Sci.* **2023**, *24* (2), No. 1438.

(21) Mendez, M. A.; Szalai, V. A. Fluorescence of unmodified oligonucleotides: a tool to probe G-quadruplex DNA structure. *Biopolymers* **2009**, *91* (10), 841−850.

(22) Friedman, S. J.; Terentis, A. C. Analysis of G-quadruplex conformations using Raman and polarized Raman spectroscopy. *J. Raman Spectrosc.* **2016**, *47* (3), 259−268.

(23) Tan, W.; Yi, L.; Zhu, Z.; Zhang, L.; Zhou, J.; Yuan, G. Hsa-miR-1587 G-quadruplex formation and dimerization induced by NH_4^+, molecular crowding environment and jatrorrhizine derivatives. *Talanta* **2018**, *179*, 337−343.

(24) Kong, J.-N.; Zhang, C.; Zhu, Y.-C.; Zhong, K.; Wang, J.; Chu, B.-B.; Yang, G.-Y. Identification and characterization of G-quadruplex formation within the EP0 promoter of pseudorabies virus. *Sci. Rep.* **2018**, *8* (1), No. 14029.

(25) Tseng, T.-Y.; Chang, T. -C.; Cheng, J.-Y. A correlation of polymorphic G-quadruplex formation in vitro and in the lysosomes of live cancer cells. *Int. J. Biol. Macromol.* **2025**, *290*, No. 138899.

(26) Qiao, J.-q.; Liang, C.; Zhu, Z.; Cao, Z.; Zheng, W.; Lian, H. Monolithic alkylsilane column: A promising separation medium for

oligonucleotides by ion-pair reversed-phase liquid chromatography. *J. Chromatogr. A* **2018**, *1569*, 168−177.
(27) Qiao, J.; Liang, C.; Wei, L.; Cao, Z.; Lian, H. Retention of nucleic acids in ion-pair reversed-phase high-performance liquid chromatography depends not only on base composition but also on base sequence. *J. Sep. Sci.* **2016**, *39* (23), 4502−4511.
(28) Liang, C.; Qiao, J.-Q.; Lian, H.-Z. A novel strategy for retention prediction of nucleic acids with their sequence information in ion-pair reversed phase liquid chromatography. *Talanta* **2018**, *185*, 592−601.
(29) Zhou, B.; Geng, Y.; Liu, C.; Miao, H.; Ren, Y.; Xu, N.; Shi, X.; You, Y.; Lee, T.; Zhu, G. Characterizations of distinct parallel and antiparallel G-quadruplexes formed by two-repeat ALS and FTD related GGGGCC sequence. *Sci. Rep.* **2018**, *8* (1), No. 2366.
(30) Chang, T.; Liu, X.; Cheng, X.; Qi, C.; Mei, H.; Shangguan, D. Selective isolation of G-quadruplexes by affinity chromatography. *J. Chromatogr. A* **2012**, *1246*, 62−68.
(31) Largy, E.; Mergny, J.-L. Shape matters: size-exclusion HPLC for the study of nucleic acid structural polymorphism. *Nucleic Acids Res.* **2014**, *42* (19), No. e149.
(32) Qiao, J.-q.; Cao, Z.; Liang, C.; Chen, H.; Zheng, W.; Lian, H. Study on the polymorphism of G-quadruplexes by reversed-phase HPLC and LC−MS. *J. Chromatogr. A* **2018**, *1542*, 61−71.
(33) Wang, J.; Qiao, J.-Q.; Zheng, W.-J.; Lian, H.-Z. Effect of ionic liquids as mobile phase additives on retention behaviors of G-quadruplexes in reversed-phase high performance liquid chromatography. *J. Chromatogr. A* **2024**, *1715*, No. 464604.
(34) Paiva, A.; Craveiro, R.; Aroso, I.; Martins, M.; Reis, R. L.; Duarte, A. R. C. Natural Deep Eutectic Solvents − Solvents for the 21st Century. *ACS Sustainable Chem. Eng.* **2014**, *2* (5), 1063−1071.
(35) Zhang, H.; Vicent-Luna, J. M.; Tao, S.; Calero, S.; Jiménez Riobóo, R. J.; Ferrer, M. L.; del Monte, F.; Gutiérrez, M. C. Transitioning from ionic liquids to deep eutectic solvents. *ACS Sustainable Chem. Eng.* **2022**, *10* (3), 1232−1245.
(36) Omar, K. A.; Sadeghi, R. Database of deep eutectic solvents and their physical properties: A review. *J. Mol. Liq.* **2023**, *384*, No. 121899.
(37) Florindo, C.; Branco, L. C.; Marrucho, I. M. Quest for green-solvent design: from hydrophilic to hydrophobic (deep) eutectic solvents. *ChemSusChem* **2019**, *12* (8), 1549−1559.
(38) Ling, J. K. U.; Hadinoto, K. Deep Eutectic solvent as green solvent in extraction of biological macromolecules: A Review. *Int. J. Mol. Sci.* **2022**, *23* (6), No. 3381.
(39) Lapeña, D.; Errazquin, D.; Lomba, L.; Lafuente, C.; Giner, B. Ecotoxicity and biodegradability of pure and aqueous mixtures of deep eutectic solvents: glyceline, ethaline, and reline. *Environ. Sci. Pollut. Res.* **2021**, *28* (7), 8812−8821.
(40) Hayyan, M.; Hashim, M. A.; Hayyan, A.; Al-Saadi, M. A.; AlNashef, I. M.; Mirghani, M. E. S.; Saheed, O. K. Are deep eutectic solvents benign or toxic? *Chemosphere* **2013**, *90* (7), 2193−2195.
(41) Zaib, Q.; Eckelman, M. J.; Yang, Y.; Kyung, D. Are deep eutectic solvents really green?: A life-cycle perspective. *Green Chem.* **2022**, *24* (20), 7924−7930.
(42) Płotka-Wasylka, J.; de la Guardia, M.; Andruch, V.; Vilková, M. Deep eutectic solvents vs ionic liquids: Similarities and differences. *Microchem. J.* **2020**, *159*, No. 105539.
(43) Garcia, M. T.; Gathergood, N.; Scammells, P. J. Biodegradable ionic liquids Part II. Effect of the anion and toxicology. *Green Chem.* **2005**, *7* (1), 9−14.
(44) Khan, A. S.; Sakina; Nasrullah, A.; Ullah, S.; Ullah, Z.; Khan, Z.; Khan, N. A.; Khan, S. Z.; Din, I. U. An overview on phytotoxic perspective of ionic liquids and deep eutectic solvents: The role of chemical structure in the phytotoxicity. *ChemBioEng. Rev.* **2023**, *10* (2), 174−194.
(45) Cho, C.-W.; Pham, T. P. T.; Zhao, Y.; Stolte, S.; Yun, Y.-S. Review of the toxic effects of ionic liquids. *Sci. Total Environ.* **2021**, *786*, No. 147309.
(46) Libralato, G.; Volpi Ghirardini, A.; Avezzù, F. Seawater ecotoxicity of monoethanolamine, diethanolamine and triethanolamine. *J. Hazard. Mater.* **2010**, *176*, 535−539.
(47) Flieger, J.; Flieger, M. Ionic Liquids Toxicity—Benefits and Threats. *Int. J. Mol. Sci.* **2020**, *21* (17), No. 6267.
(48) Santana-Mayor, Á.; Rodríguez-Ramos, R.; Herrera-Herrera, A. V.; Socas-Rodríguez, B.; Rodríguez-Delgado, M. Á. Deep eutectic solvents. The new generation of green solvents in analytical chemistry. *Trends Anal. Chem.* **2021**, *134*, No. 116108.
(49) Shishov, A.; El-Deen, A. K.; Godunov, P.; Bulatov, A. Atypical deep eutectic solvents: New opportunities for chemical analysis. *Trends Anal. Chem.* **2024**, *176*, No. 117752.
(50) Liu, Q.; Wei, W.; Liu, Y.; Zhang, Y.; Chen, W.; Tang, S. Deep eutectic supramolecular polymers based HPLC stationary phase: Green synthesis strategy and promising application prospects. *Anal. Chim. Acta* **2024**, *1330*, No. 343268.
(51) Płotka-Wasylka, J.; Rutkowska, M.; de la Guardia, M. Are deep eutectic solvents useful in chromatography? A short review. *J. Chromatogr A* **2021**, *1639*, No. 461918.
(52) Sutton, A. T.; Fraige, K.; Leme, G. M.; da Silva Bolzani, V.; Hilder, E. F.; Cavalheiro, A. J.; Arrua, R. D.; Funari, C. S. Natural deep eutectic solvents as the major mobile phase components in high-performance liquid chromatography—searching for alternatives to organic solvents. *Anal. Bioanal. Chem.* **2018**, *410* (16), 3705−3713.
(53) Berthod, A.; Ruiz-Ángel, M. J.; Carda-Broch, S. Recent advances on ionic liquid uses in separation techniques. *J. Chromatogr A* **2018**, *1559*, 2−16.
(54) He, S.; Choi, D. M.; Row, K. H. Utilization of ionic deep eutectic solvent as sustainable mobile phase additive in high-performance liquid chromatography for improving the separation of biogenic amines. *J. Sep. Sci.* **2022**, *45* (22), 4005−4011.
(55) Tan, T.; Zhang, M.; Wan, Y.; Qiu, H. Utilization of deep eutectic solvents as novel mobile phase additives for improving the separation of bioactive quaternary alkaloids. *Talanta* **2016**, *149*, 85−90.
(56) Jiang, Z.-M.; Liu, W.-J.; Li, Y.; Liu, J.; Wang, H.-Y.; Li, P.; Liu, E.-H. Eco-friendly deep eutectic solvents contribute to improving the separation of isoquinoline alkaloids in supercritical fluid chromatography. *ACS Sustainable Chem. Eng.* **2020**, *8* (36), 13777−13783.
(57) Gao, F.; Liu, L.; Tang, W.; Row, K. H.; Zhu, T. Optimization of the chromatographic behaviors of quercetin using choline chloride-based deep eutectic solvents as HPLC mobile-phase additives. *Sep. Sci. Technol.* **2018**, *53* (2), 397−403.
(58) Li, G.; Zhu, T.; Lei, Y. Choline chloride-based deep eutectic solvents as additives for optimizing chromatographic behavior of caffeic acid. *Korean J. Chem. Eng.* **2015**, *32* (10), 2103−2108.
(59) Macaya, R. F.; Schultze, P.; Smith, F. W.; Roe, J. A.; Feigon, J. Thrombin-binding DNA aptamer forms a unimolecular quadruplex structure in solution. *Proc. Natl. Acad. Sci. U.S.A.* **1993**, *90* (8), 3745−3749.
(60) Schultze, P.; Macaya, R. F.; Feigon, J. Three-dimensional solution structure of the thrombin-binding DNA aptamer d(GGTTGGTGTGGTTGG). *J. Mol. Biol.* **1994**, *235* (5), 1532−1547.
(61) Reshetnikov, R.; Golovin, A.; Spiridonova, V.; Kopylov, A.; Šponer, J. Structural dynamics of thrombin-binding DNA aptamer d(GGTTGGTGTGGTTGG) Quadruplex DNA studied by large-scale explicit solvent simulations. *J. Chem. Theory Comput.* **2010**, *6* (10), 3003−3014.
(62) Mao, X.-a.; Gmeiner, W. H. NMR study of the folding−unfolding mechanism for the thrombin-binding DNA aptamer d(GGTTGGTGTGGTTGG). *Biophys. Chem.* **2005**, *113* (2), 155−160.
(63) Luu, K. N.; Phan, A. T.; Kuryavyi, V.; Lacroix, L.; Patel, D. J. Structure of the human telomere in K^+ Solution: An intramolecular (3 + 1) G-quadruplex scaffold. *J. Am. Chem. Soc.* **2006**, *128* (30), 9963−9970.
(64) Bessi, I.; Jonker, H. R. A.; Richter, C.; Schwalbe, H. Involvement of long-lived intermediate states in the complex folding pathway of the human telomeric G-quadruplex. *Angew. Chem., Int. Ed.* **2015**, *54* (29), 8444−8448.

https://doi.org/10.1021/acs.analchem.5c08145
Anal. Chem. 2026, 98, 16083−16095

(65) Rauser, V.; Weinhold, E. Quantitative formation of monomeric G-Quadruplex DNA from multimeric structures of c-Myc promoter sequence. *ChemBioChem* **2020**, *21* (17), 2445−2448.
(66) Ambrus, A.; Chen, D.; Dai, J.; Jones, R. A.; Yang, D. Solution structure of the biologically relevant G-quadruplex element in the human c-MYC promoter. Implications for G-quadruplex stabilization. *Biochemistry* **2005**, *44* (6), 2048−2058.
(67) Lim, K. W.; Lacroix, L.; Yue, D. J. E.; Lim, J. K. C.; Lim, J. M. W.; Phan, A. T. Coexistence of two distinct G-quadruplex conformations in the hTERT Promoter. *J. Am. Chem. Soc.* **2010**, *132* (35), 12331−12342.
(68) Phan, A. T.; Patel, D. J. Two-repeat human telomeric d(TAGGGTTAGGGT) Sequence forms interconverting parallel and antiparallel g-quadruplexes in solution: distinct topologies, thermodynamic properties, and folding/unfolding kinetics. *J. Am. Chem. Soc.* **2003**, *125* (49), 15021−15027.
(69) Dailey, M. M.; Miller, M. C.; Bates, P. J.; Lane, A. N.; Trent, J. O. Resolution and characterization of the structural polymorphism of a single quadruplex-forming sequence. *Nucleic Acids Res.* **2010**, *38* (14), 4877−4888.
(70) Lee, P. C.; Melsel, D. Adsorption and surface-enhanced Raman of dyes on silver and gold sols. *J. Phys. Chem. A* **1982**, *86* (17), 3391−3395.
(71) Maestro - Schrödinger, LLC, 2015.
(72) Jorgensen, W. L.; Maxwell, D. S.; Tirado-Rives, J. Development and testing of the OPLS all-atom force field on conformational energetics and properties of organic liquids. *J. Am. Chem. Soc.* **1996**, *118* (45), 11225−11236.
(73) Friesner, R. A.; Banks, J. L.; Murphy, R. B.; Halgren, T. A.; Klicic, J. J.; Mainz, D. T.; Repasky, M. P.; Knoll, E. H.; Shelley, M.; Perry, J. K.; Shaw, D. E.; Francis, P.; Shenkin, P. S. Glide: A new approach for rapid, accurate docking and scoring. 1. method and assessment of docking accuracy. *J. Med. Chem.* **2004**, *47* (7), 1739−1749.
(74) Halgren, T. A.; Murphy, R. B.; Friesner, R. A.; Beard, H. S.; Frye, L. L.; Pollard, W. T.; Banks, J. L. Glide: A new approach for rapid, accurate docking and scoring. 2. Enrichment factors in database screening. *J. Med. Chem.* **2004**, *47* (7), 1750−1759.
(75) Yusof, R.; Jumbri, K.; Ahmad, H.; Abdulmalek, E.; Abdul Rahman, M. B. Binding of tetrabutylammonium bromide based deep eutectic solvent to DNA by spectroscopic analysis. *Spectrochim. Acta, Part A* **2021**, *253*, No. 119543.
(76) Zhao, C.; Ren, J.; Qu, X. G-Quadruplexes form ultrastable parallel structures in deep eutectic solvent. *Langmuir* **2013**, *29* (4), 1183−1191.
(77) Feng, B.; Sosa, R. P.; Mårtensson, A. K. F.; Jiang, K.; Tong, A.; Dorfman, K. D.; Takahashi, M.; Lincoln, P.; Bustamante, C. J.; Westerlund, F.; Nordén, B. Hydrophobic catalysis and a potential biological role of DNA unstacking induced by environment effects. *Proc. Natl. Acad. Sci. U. S. A.* **2019**, *116* (35), 17169−17174.
(78) Li, Y.; Han, X.; Zhou, S.; Yan, Y.; Xiang, X.; Zhao, B.; Guo, X. Structural features of DNA G-Quadruplexes revealed by surface-enhanced Raman spectroscopy. *J. Phys.Chem. Lett.* **2018**, *9* (12), 3245−3252.
(79) Miljanić, S.; Ratkaj, M.; Matković, M.; Piantanida, I.; Gratteri, P.; Bazzicalupi, C. Assessment of human telomeric G-quadruplex structures using surface-enhanced Raman spectroscopy. *Anal. Bioanal. Chem.* **2017**, *409* (9), 2285−2295.
(80) Rusciano, G.; De Luca, A. C.; Pesce, G.; Sasso, A.; Oliviero, G.; Amato, J.; Borbone, N.; D'Errico, S.; Piccialli, V.; Piccialli, G.; Mayol, L. Label-Free Probing of G-quadruplex formation by surface-enhanced Raman scattering. *Anal. Chem.* **2011**, *83* (17), 6849−6855.
(81) Breuzard, G.; Millot, J.-M.; Riou, J.-F.; Manfait, M. Selective interactions of ethidiums with G-quadruplex DNA revealed by surface-enhanced Raman scattering. *Anal. Chem.* **2003**, *75* (16), 4305−4311.
(82) Xu, L.-J.; Lei, Z.-C.; Li, J.; Zong, C.; Yang, C. J.; Ren, B. Label-free surface-enhanced Raman spectroscopy detection of DNA with single-base sensitivity. *J. Am. Chem. Soc.* **2015**, *137* (15), 5149−5154.
(83) Cao, Y.; Ding, P.; Yang, L.; Li, W.; Luo, Y.; Wang, J.; Pei, R. Investigation and improvement of catalytic activity of G-quadruplex/hemin DNAzymes using designed terminal G-tetrads with deoxyadenosine caps. *Chem. Sci.* **2020**, *11* (26), 6896−6906.

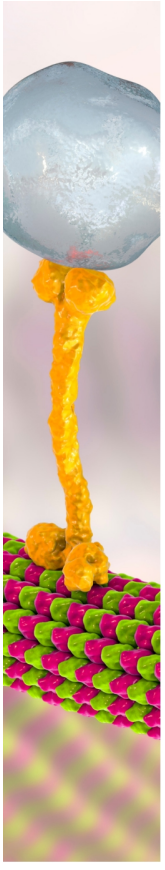

https://doi.org/10.1021/acs.analchem.5c08145
Anal. Chem. 2026, 98, 16083−16095